

Mindanao Current/Undercurrent in an eddy-resolving GCM

Tangdong Qu,¹ Tzu-Ling Chiang,^{1,2} Chau-Ron Wu,² Pierre Dutrieux,^{3,4} and Dunxin Hu⁵

Received 15 December 2011; revised 23 March 2012; accepted 22 May 2012; published 29 June 2012.

[1] Analysis of results from an eddy-resolving general circulation model showed two subsurface velocity cores in the mean within the depth range between 400 and 1000 m below the Mindanao Current (MC). One is confined to the inshore edge at about 126.8°E and connected with the Sulawesi Sea. The other takes place somewhat offshore around 127.7°E, being closely related to the intrusion of South Pacific water. Both cores are referred to as the Mindanao Undercurrent (MUC). The MC/MUC is approximately a geostrophic flow, except on the inshore edge of the MUC where up to 50% of the mean flow can be explained by ageostrophic dynamics. In contrast with the well-defined southward flowing MC, the MUC is of high velocity variance relative to the mean. Empirical orthogonal function (EOF) analysis shows that approximately 60% of the total velocity variance is associated with two meandering modes, with their major signatures in the subthermocline. The dominant time scale of variability is 50–100 days. An ensemble of these meso-scale fluctuations provides a northward freshwater flux on the offshore edge of the Philippine coast, which to a certain extent explains why water of South Pacific origin appears to extend farther northward than the mean MUC. In the offshore velocity core of the MUC, for example, eddy induced freshwater flux is equivalent to a mean flow of about 0.3 m s⁻¹ in the density range between 26.9 and 27.3 kg m⁻³, which is greater than the mean current by a factor of 6.

Citation: Qu, T., T.-L. Chiang, C.-R. Wu, P. Dutrieux, and D. Hu (2012), Mindanao Current/Undercurrent in an eddy-resolving GCM, *J. Geophys. Res.*, 117, C06026, doi:10.1029/2011JC007838.

1. Introduction

[2] The North Equatorial Current (NEC) bifurcates as it approaches the Philippine coast, with its southern branch forming the Mindanao Current (MC) and northern branch constituting the Kuroshio [e.g., Nitani, 1972; Toole *et al.*, 1990; Lukas *et al.*, 1996; Qu and Lukas, 2003; Wang and Hu, 2006]. Most of the Kuroshio bypasses the Luzon Strait and flows northward along the continental slope east of China [e.g., Lee *et al.*, 2001], with only a small fraction intruding into the South China Sea (SCS) [Wyrki, 1961]. A substantial portion of the MC flows into the Sulawesi Sea to feed the Indonesian Throughflow, while the rest makes its way directly into the North Equatorial Countercurrent (NECC) [Wyrki, 1961; Lukas *et al.*, 1991].

[3] Underlying the Kuroshio, a southward subsurface flow, known as the Luzon Undercurrent (LUC) [Qu *et al.*, 1997], was observed during the Tropical Ocean and Global Atmosphere program (TOGA) [Hu and Cui, 1991]. With multiyear conductivity-temperature-depth (CTD) observations, this subsurface flow was shown to start at depths below about 500 m near 22°N, reflecting the northward shift of the NEC bifurcation with increasing depth [Qu and Lukas, 2003]. The undercurrent intensifies southward and eventually becomes part of the MC off the Mindanao coast, providing a pathway for North Pacific waters to enter the equatorial region [Fine *et al.*, 1994; Bingham and Lukas, 1995; Qu and Lukas, 2003].

[4] An undercurrent below the MC was also reported [e.g., Hu and Cui, 1989; Hu *et al.*, 1991]. Based on three CTD transects off the Mindanao coast near 7.5°N, Hu and Cui [1989] found multiple northward velocity cores below about 500 m and named them the Mindanao Undercurrent (MUC). This undercurrent structure was visible in the acoustic Doppler current profile (ADCP) measurements collected during the Western Equatorial Pacific Ocean Circulation Study (WEPOCS) [Lukas *et al.*, 1991], showing that the MUC is 20–25 km wide and 50–75 km offshore. Several analyses of hydrographic data further suggested that, although its intensity and location vary from time to time, the MUC is a quasi-permanent feature [e.g., Wang and Hu, 1998a; Qu *et al.*, 1999]. In an analysis of seven ADCP transects taken between 1987 and 1990, however, Wijffels *et al.* [1995] noted that the subsurface flow underlying the

¹International Pacific Research Center, SOEST, University of Hawai'i at Mānoa, Honolulu, Hawaii, USA.

²Department of Earth Sciences, National Taiwan Normal University, Taipei, Taiwan.

³Department of Oceanography, SOEST, University of Hawai'i at Mānoa, Honolulu, Hawaii, USA.

⁴Now at Physical Science Division, British Antarctic Survey, Cambridge, UK.

⁵Institute of Oceanology, Chinese Academy of Sciences, Qingdao, China.

Corresponding author: T. Qu, International Pacific Research Center, SOEST, University of Hawai'i at Mānoa, 1680 East-West Rd., Honolulu, HI 96822, USA. (tangdong@hawaii.edu)

MC is highly variable, and this led them to a speculation that the MUC is merely a transient phenomenon.

[5] Studies of the MC/MUC have focused on its seasonal to interannual variability, in response to local changes in the wind [e.g., *Wyrski*, 1961], as well as to remote changes through the westward propagation of Rossby waves [e.g., *Kessler*, 1990, *Masumoto and Yamagata*, 1991; *Qiu and Lukas*, 1996; *Tozuka et al.*, 2002]. Among others, *Lukas* [1988] analyzed the daily sea level data from Davao and Malakal and inferred that the MC/MUC transport contains a strong, intermittent quasi-biennial signal. Recent studies also revealed the existence of annual and semiannual signals in the MC/MUC transport [e.g., *Tozuka et al.*, 2002; *Qu et al.*, 2008; *Kashino et al.*, 2011]. On interannual time scale, the current was shown to correspond well with El Niño–Southern Oscillation (ENSO) [e.g., *Kim et al.*, 2004; *Kashino et al.*, 2009, 2011].

[6] The western Pacific Ocean is populated with high-frequency fluctuations and/or meso-scale eddies, due to the region's complex coastal geometry and the ocean's intrinsic instability. As a ubiquitous feature in the ocean [*Kessler*, 2005; *Chelton et al.*, 2007], the surface expression of meso-scale eddies accounts for a significant fraction of variability in sea surface height and may exert strong influence on the western boundary current [e.g., *Zhang et al.*, 2001; *Wu and Chiang*, 2007; *Hsin et al.*, 2010]. Most of these earlier studies, however, focused on the surface layer, and so far eddy activities in the subthermocline of the region have remained largely unexplored. Off the Mindanao coast, direct measurements from a single mooring taken from 1999 to 2002 indicated that the circulation below and offshore the MC was dominated by eddy activities. Based on lowered ADCP measurements from two individual cruises, *Firing et al.* [2005] further suggested that the northward flow below and offshore the MC was actually part of a set of subthermocline eddies within about 300 km of the coast. Then, the questions that may arise immediately are (1) whether or not the MUC is a robust flow and (2) what precise role meso-scale eddies can play in the MC/MUC. Due to the lack of sufficient observations, these questions have never been carefully examined. Taking advantage of the rapid advance in ocean modeling, this study investigates the detailed structure, dominant scale of variability, and generating mechanism of the MC/MUC in an eddy-resolving Ocean General Circulation Model (OGCM).

[7] The rest of the paper is organized as follows. After a brief model description in section 2, we present some general characteristics of the region simulated by the model in section 3. We focus our investigation on the MC/MUC in section 4. The mechanisms that govern the MC/MUC are investigated in section 5. Eddy activities and their impacts on salinity distribution are discussed in section 6. Results are summarized in section 7.

2. Model Description

[8] The model used for the present study is the OGCM for the Earth Simulator (OFES). It was based on the Modular Ocean Model (MOM3), with spherical grid in horizontal and z-coordinate in vertical, respectively. Its domain covers a near-global region extending from 75°S to 75°N, with a horizontal resolution of 0.1 degree both in longitude and

latitude. The vertical resolution varies from 5 m near the surface to 330 m near the bottom, with a total of 54 levels. The model topography was constructed from a 1/30° bathymetry data set created by the Ocean Circulation and Climate Advanced Modeling Project (OCCAM) at the Southampton Oceanography Center, being able to resolve most detailed topographic features in the region studied (figure not shown).

[9] A 50-year climatological spin-up was first executed from annual mean temperature and salinity fields of the World Ocean Atlas 1998 (WOA98). Then, the model was forced from 1950 to 2008 with daily surface wind stress, heat flux, and salinity flux based on the NCEP re-analysis products. The surface fluxes were specified with bulk formula from the re-analyzed atmospheric variables, in addition to a surface salinity restoring to the climatological value of WOA98. To suppress grid-scale noises, a scale-selective damping of bi-harmonic operator was adopted for horizontal mixing, and the K-Profile Parameterization (KPP) scheme was employed for the vertical mixing. The 3-day snapshot model outputs for the period 1980–2008 are used for the present analysis. The readers are referred to *Masumoto et al.* [2004] and *Sasaki et al.* [2004] for more details about the configuration and evaluation of this model.

3. General Characteristics of the Region's Circulation

[10] With its high resolution and realistic topography, OFES was able to reproduce most observed phenomena over the global ocean, suggesting that the circulation from OFES is one of the best available in a model [*Masumoto et al.*, 2004; *Sasaki et al.*, 2004]. In the far western tropical Pacific, *Dutrieux* [2009] recently compared the model results with a new collection of shipboard ADCP measurements, and suggested that the model represents reasonably well the region's circulation and its variability. To gain further insight into the model's behavior in simulating the low-latitude western boundary current, we examine current structure and property distribution in the region 115°E–140°E and 0°N–20°N below.

[11] Near the surface (108 m), the simulation clearly demonstrates the circulation pattern described in section 1 (Figure 1a). In the mean, the model's NEC bifurcation occurs at about 15°N, coinciding with the zonally integrated wind stress curl line [e.g., *Qu and Lukas*, 2003]. From there, the NEC splits into the northward flowing Kuroshio and southward flowing MC along the western boundary. As already noted by earlier studies, current in the region is fairly robust near the surface. The Kuroshio is relatively weak at its beginning but gradually gets stronger as it flows northward. The MC approaches its maximum strength near 7°N, with its mean velocity exceeding 1.2 m s⁻¹ near the surface. The mean transports of the two currents within the depth range from the surface to 1500 m and longitude band from the coast to 130°E reach 14.9 Sv at 18°N and 23.9 Sv at 8°N, respectively, showing a reasonable agreement with earlier observations [e.g., *Nitani*, 1972; *Qu et al.*, 1998].

[12] The velocity variance of the current is generally low relative to the mean near the surface. At 108 m, for example, the standard deviation (STD) of velocity is well below 20% of its mean value over the period of integration (Figure 1b).

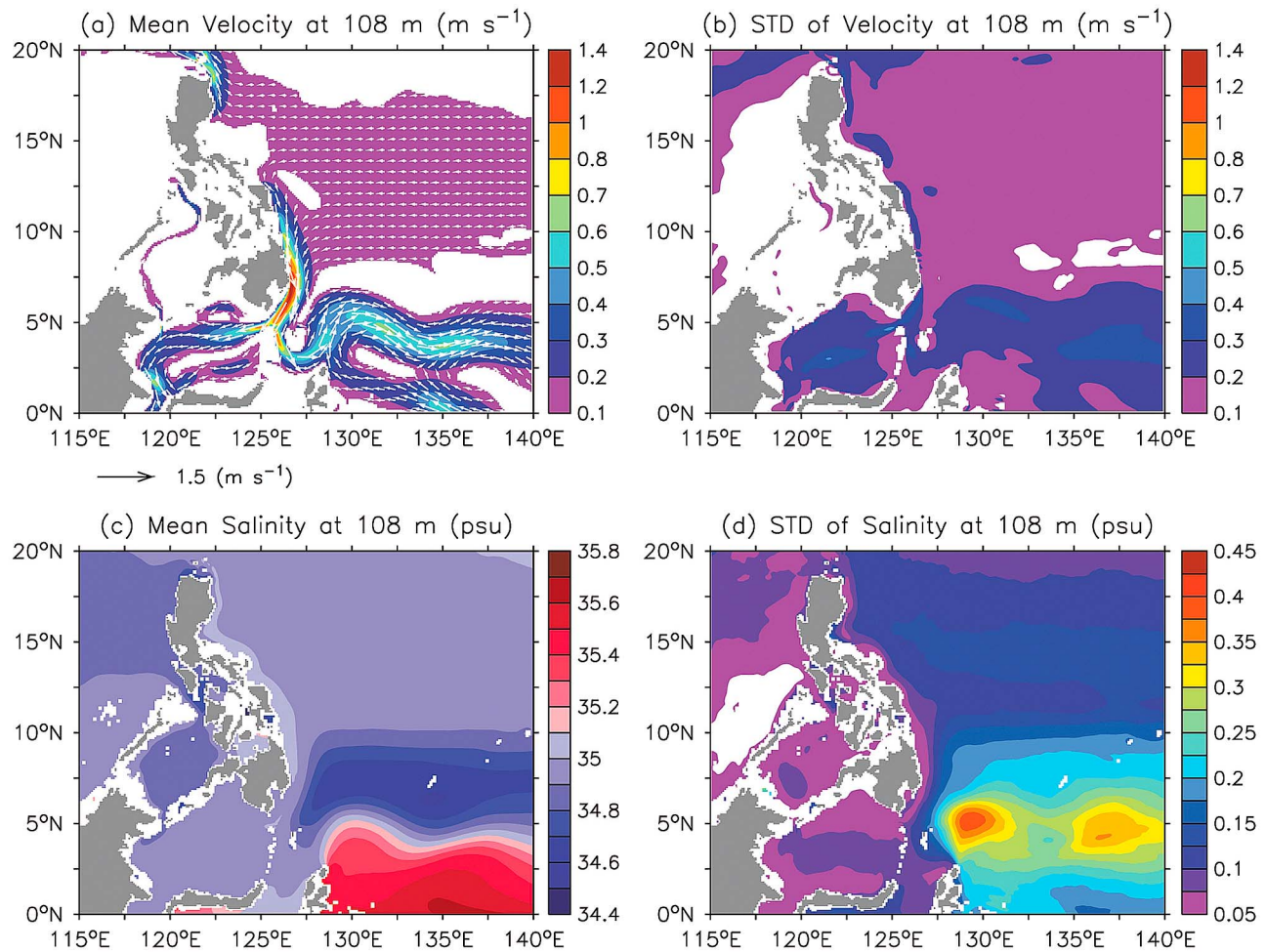


Figure 1. (a and c) Mean and (b and d) STD of velocity (Figures 1a and 1b) and salinity (Figures 1c and 1d) at 108 m from the model. Shading in Figures 1a and 1b indicates the magnitude of velocity.

In the MC, the typical STD is about 0.2 m s^{-1} , which is consistent with earlier observations [Wijffels *et al.*, 1995; Kashino *et al.*, 2005, 2009; Dutrieux, 2009]. The largest STD occurs in the NECC region, where it reaches about the same magnitude as the mean current. As a crossroad of water masses [e.g., Fine *et al.*, 1994], the region is characterized by high salinity ($>34.8 \text{ psu}$) water from both hemispheres, reflecting the intrusion of South and North Pacific Tropical Waters [e.g., Lindstrom *et al.*, 1987; Tsuchiya, 1991; Qu *et al.*, 1999]. Lying between about 5°N and 10°N , a relatively low ($<34.6 \text{ psu}$) salinity tongue is seen extending from the central Pacific (Figure 1c). The convergence of these water masses forms a salinity front at about 5°N , where its STD exceeds 0.3 psu (Figure 1d).

[13] The mean current structure changes as we proceed to deeper levels. At 605 m , the MC is nearly invisible, and the mean current off Mindanao is predominantly northward (Figure 2a). A prominent feature of this northward flow is related to an anti-cyclonic eddy southeast of Mindanao. This anti-cyclonic eddy was previously reported. Qu *et al.* [1999] suggested that it is a result of poleward tilt of Halmahera Eddy in the subthermocline. The model's vorticity distribution confirms this earlier speculation (figure not shown). Water of South Pacific origin with salinity less than 34.5 psu

extends northward from the Coral Sea (Figure 2c), as part of the New Guinea Coastal Undercurrent (NGCUC) [Lindstrom *et al.*, 1987]. Some fraction of the South Pacific water joins the anti-cyclonic eddy off Mindanao and continues northward on its western side. The northward flow of the South Pacific water can reach about 12°N along the Philippine coast, and then most of it turns eastward into the interior ocean. These characteristics match Hu and Cui's [1989, 1991], Wang *et al.*'s [1998], and Qu *et al.*'s [1999] results well, and correspond to the undercurrent below the NEC [Hu and Cui, 1989, 1991; Wang *et al.*, 1998].

[14] The velocity variance relative to the mean is high at 605 m (Figure 2b). Its STD often exceeds 0.2 m s^{-1} and can be as large as 0.3 m s^{-1} near the Mindanao coast. An offshore maximum is seen at about 12°N , coinciding roughly with the northern boundary of the MUC [e.g., Hu and Cui, 1989, 1991; Wang *et al.*, 1998; Qu *et al.*, 1999]. This STD maximum is larger than the mean velocity by a factor of about 5, lending additional support for the speculations on strong eddy activities in the region [Wijffels *et al.*, 1995; Firing *et al.*, 2005; Kashino *et al.*, 2005]. The STD of velocity is somewhat smaller elsewhere, and seems to have a comparable strength with the mean current near the New Guinea-Halmahera coast. Mean salinity attains its maximum

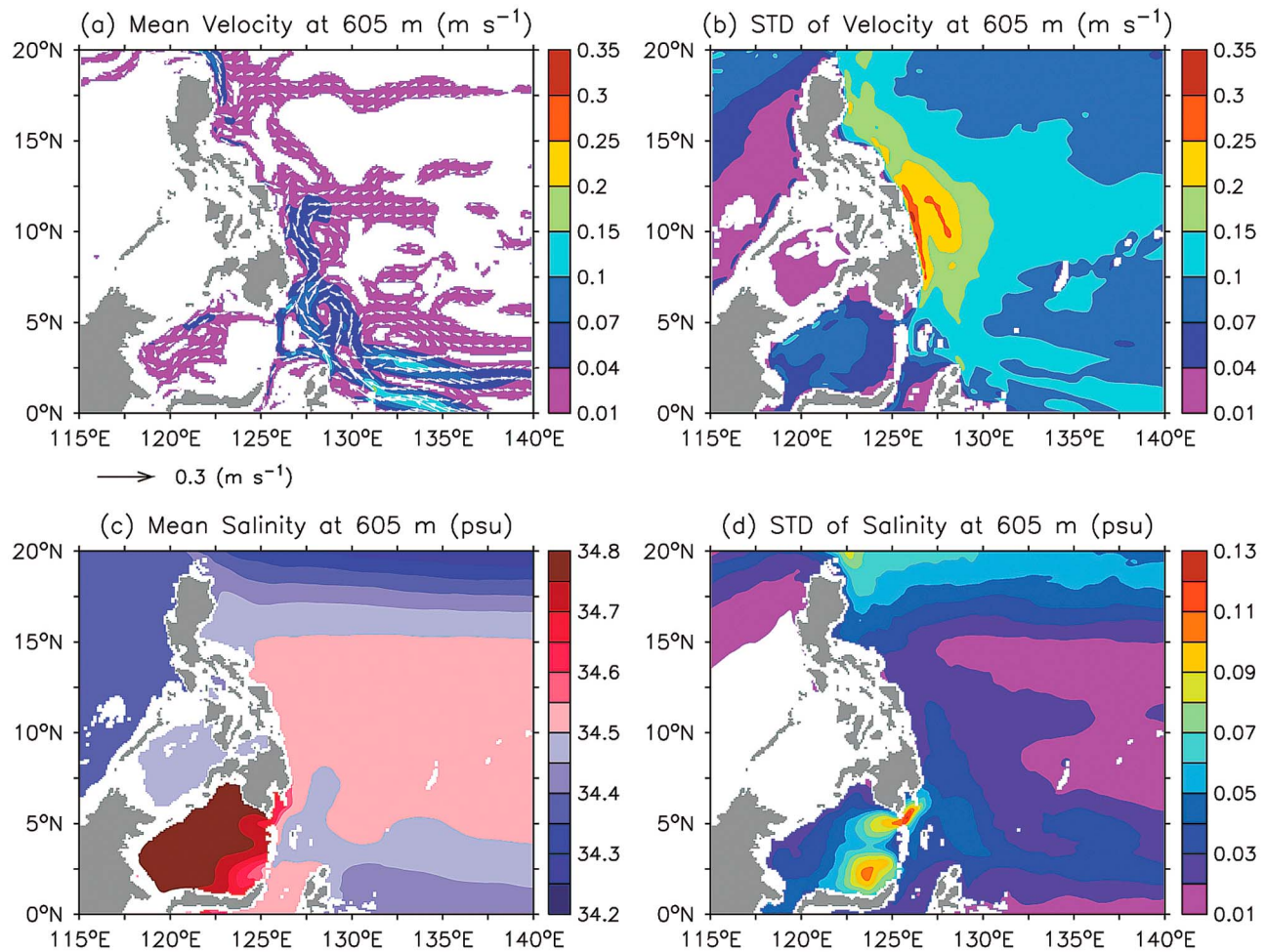


Figure 2. Same as Figure 1 except at 605 m.

(~ 34.8 psu) in the Sulawesi Sea (Figure 2c), forming a salinity front with the intrusion of low salinity water from the South Pacific. Associated with this salinity front is a STD maximum exceeding 0.1 psu, typically larger than that elsewhere by a factor of 2 (Figure 2d).

4. Mindanao Current/Undercurrent

4.1. Mean Structure

[15] Meridional velocity at 7°N shows a detailed structure of the mean MC/MUC (Figure 3). Qualitatively, the MC/MUC is well simulated by OFES, with an intensive southward flow near the surface overlying weaker northward flows in the 400–1000 m depth range. In the mean, the meridional velocity consists of two subthermocline cores (Figure 3a). One hugs the coast near 126.8°E and the other lies somewhat offshore at about 127.7°E , with a maximum velocity of about 0.05 m s^{-1} at 600–700 m depth. Both cores are referred to as the MUC in the following discussion.

[16] The multiple northward velocity cores below and offshore the MC were first reported by *Hu and Cui* [1989], based on three CTD transactions off Mindanao. Despite considerable variations, the multicore structure was also visible in the CTD and ADCP observations from WEPOCS [*Lukas et al.*, 1991, Figures 6e and 7c]. The most remarkable

evidence was recently provided by the lower ADCP measurements of R/V *Mirai* (Y. Kashino, personal communication, 2012). In particular, both velocity cores below 500 m were captured in the MR11–06 cruise (figure available in *Mirai Cruise Report* at http://docsrv.godac.jp/MSV2_DATA/23/MR11-06_all.pdf). All these synoptic observations seem to suggest that, though highly variable, the multicore structure of the MUC is real.

[17] The observational evidence for the mean structure of the MUC was provided by *Qu et al.* [1998] and *Wang and Hu* [1998a]. By averaging 11 CTD transactions at 7°N – 8°N , *Qu et al.* [1998] showed a similar pattern of velocity (their Figures 4c, 6b, and 7b) as we present here (Figure 3). The most striking discrepancy is that the inshore velocity core of the MUC was not visible in the observations. We speculate that the spatial scale (0.5° longitude) they used in averaging the data was not sufficient to resolve this narrow coastal flow via geostrophy. This needs to be confirmed as more high resolution data become available in the region. Another possible interpretation is related to eddy activities, and this will be discussed in section 5.

[18] The inshore velocity core of the MUC is of high variance; its STD can reach as large as 0.25 m s^{-1} (Figure 3b), exceeding its mean value by a factor of about 5. The offshore velocity core lies roughly between two STD

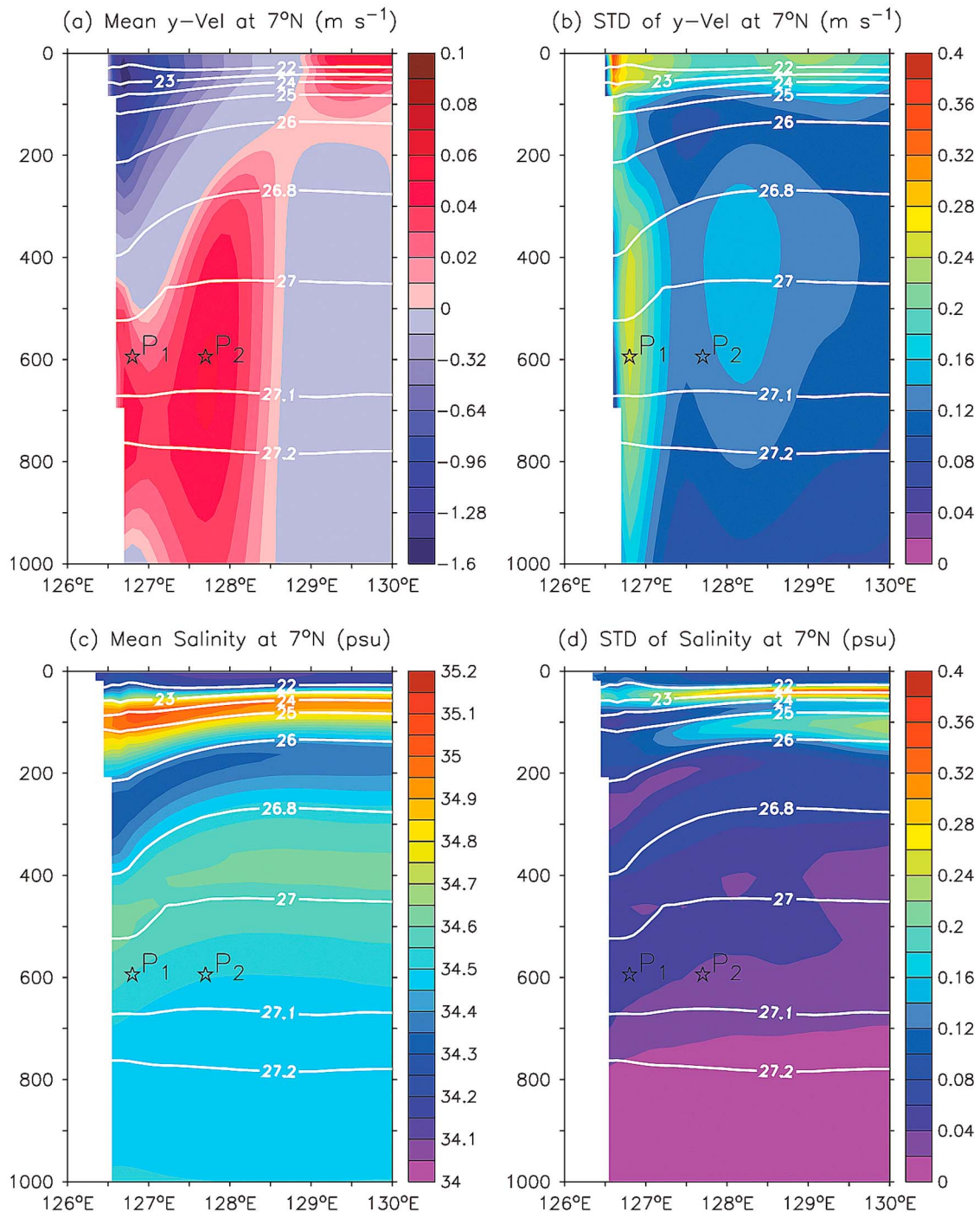


Figure 3. (a and c) Mean and (b and d) STD of meridional velocity (Figures 3a and 3b) and salinity (Figures 3c and 3d) at 7°N. The white contours indicate isopycnal surfaces (kg m^{-3}). The stars show the locations of MUC velocity cores at 126.8°E (P1) and 127.7°E (P2).

maxima, but its STD is still significantly larger than its mean value. The STD in the MC is somewhat higher ($\sim 0.35 \text{ m s}^{-1}$). As this high value is narrowly confined to the inshore edge of the western boundary in about 100 m of the surface, it can only account for a small fraction of velocity variance across the section. The highly variable nature of the MUC is also examined at other latitudes between 7°N and 10°N. As an example, Figure 4 shows the meridional velocity and its variability at 9°N. Despite some

quantitative discrepancies, it shows essentially the same pattern of variability as discussed above.

[19] Careful examination of water property distribution indicates that the offshore velocity core of the MUC is characterized by lower ($\sim 34.5 \text{ psu}$) salinity than the inshore core (Figure 3). As one can see from Figure 2, the inshore velocity core seems to have a strong connection with the Sulawesi Sea, from where relatively high salinity water is conveyed northward along the Mindanao coast. On the

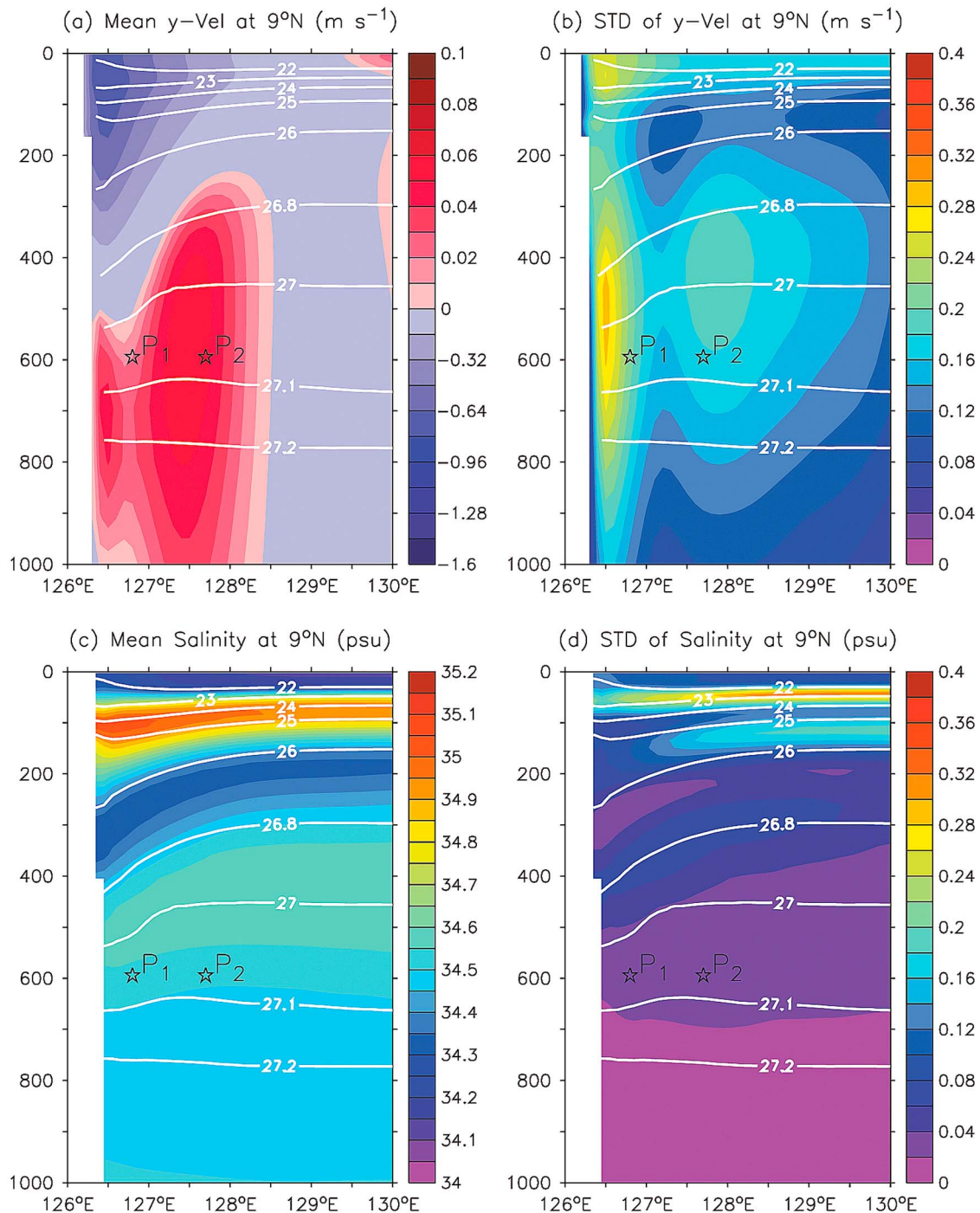


Figure 4. Same as Figure 3 except at 9°N.

contrary, the offshore velocity core represents the northward intrusion of low salinity water from the South Pacific. Some portion of the South Pacific water may enter the Sulawesi Sea and get saltier before joining the MUC along the Mindanao coast (Figure 2a). Both velocity cores lie at about $\sigma_\theta = 27.0\text{--}27.1 \text{ kg m}^{-3}$ surface, close to the density range of AAIW in the region studied [e.g., Reid, 1965; Qu *et al.*, 1999]. This result confirms that the MUC does play a role in conveying the Antarctic Intermediate Water (AAIW) toward the western North Pacific [e.g., Hu *et al.*, 1991; Fine

et al., 1994; Wang and Hu, 1997, 1998b]. Integrating over the 400–1000 m depth range from the coast to 128.5°E at 7°N, we obtain a net volume transport of 3.8 Sv. Of this transport, about 0.5 Sv is associated with the inshore velocity core (from the coast to 127.0°E) and about 3.3 Sv associated with the offshore velocity core (from 127.0°E to 128.5°E). So, in the mean, a large portion of the MUC water has a South Pacific origin, in good agreement with earlier studies based on synoptic observations [e.g., Wang and Hu, 1997].

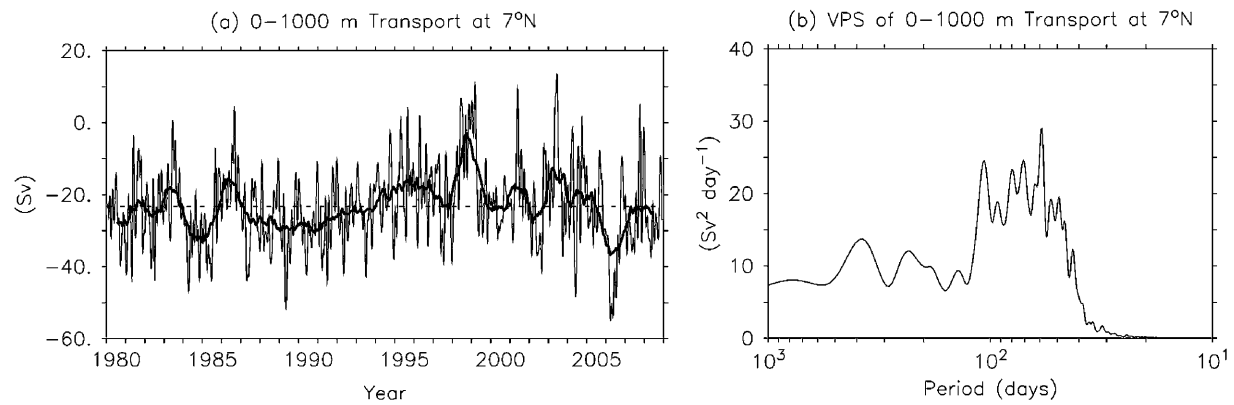


Figure 5. (a) Volume transport of the MC/MUC and (b) its variance conserving spectra in the depth range from the surface to 1000 m and longitude band from the coast to 130°E at 7°N. The heavy solid line represents variability smoothed by a 13-month running mean filter.

4.2. Transport Variability

[20] In the only available mooring observations, *Kashino et al.* [2005] have shown that the region's current variability has a dominant time scale of 25–100 days. This variability is well captured by OFES. At 7°N, the 0–1000 m integrated transport variability in the MC/MUC is dominated by fluctuations from 50 to 100 days (Figure 5). This time scale is somewhat shorter than that in the Kuroshio/LUC transport [e.g., *Johns et al.*, 2001; *Zhang et al.*, 2001], presumably due to the fact that eddies propagate faster at lower latitudes than those at higher latitudes. Similar variability in the western part of the NEC and the Sulawesi Sea surface current has been reported in previous studies [e.g., *Kashino et al.*, 1999; *Qiu et al.*, 1999; *Tozuka et al.*, 2002; *Dutrieux*, 2009]. Since the region hosts the strongest surface wind signal of the Madden-Julian oscillation [*Madden and Julian*, 1994] the intraseasonal variability in the MC/MUC transport could be directly wind-driven. However, given the complicated geometry and topography of the region, this intraseasonal variability could also be forced by instabilities of large scale circulation [*Dutrieux*, 2009].

[21] Being closely related to the annual fluctuation of Mindanao Dome [e.g., *Masumoto and Yamagata*, 1991; *Tozuka et al.*, 2002], the MC/MUC transport is maximum in early summer and minimum in fall (Figure 6), consistent with the results from earlier observations [*Wyrki*, 1961; *Qu et al.*, 1998; *Kashino et al.*, 2005]. Most of this seasonal signal is confined to the MC, and no significant seasonal variation is seen in the MUC (figure not shown). On the interannual time scale, the transport variability (Figure 5) from the model does show a signature of ENSO as previously reported [e.g., *Kim et al.*, 2004; *Kashino et al.*, 2009], but its correlation with the Southern Oscillation Index (SOI) is relatively low (0.24). In a similar calculation based on results from a 1/4°-resolution model, *Kim et al.* [2004] found a correlation of 0.54. They related the MC/MUC transport variability to the meridional migration of the NEC bifurcation and suggested that the MC gets stronger (weaker) during El Niño (La Niña) years, when the NEC bifurcation shifts northward (southward). Observational evidence for this interannual variability was recently provided by *Kashino et al.* [2009]. Based on two onboard observation campaigns,

they showed that the MC transport measured in late 2006 under the El Niño condition was stronger than that measured during early 2008 under the La Niña condition, lending support for *Kim et al.*'s [2004] result. The details require further investigation.

4.3. Dominant Modes

[22] Empirical orthogonal function (EOF) analysis is performed to characterize the variance of meridional velocity and its dominant modes in the MC/MUC. A 30-day low-pass filter is applied before the analysis to remove influences of higher frequency variability. The leading EOF mode captures about 38% of the total variance, and is dominated by meandering motions (Figure 7a). The mode consists of anti-phase variations with a zero line lying at about 127.6°E. In the west, the maximum variability is seen at about 126.8°E, coinciding with the inshore velocity core of the MUC, while in the east the maximum variability explains much of the variance at about 128.4°E (Figure 3b). A positive principal component (PC) value of this mode represents an inshore meander of the current, which enhances the velocity core on the inshore edge, and vice versa. The time evolution of PC₁ shows rapid and large onshore/offshore

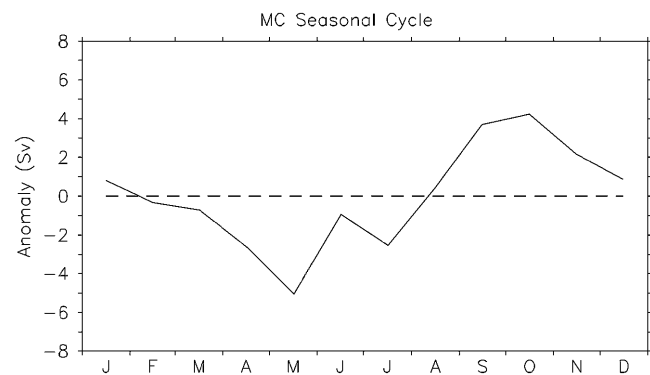


Figure 6. Mean seasonal cycle of MC/MUC transport in the depth range from the surface to 1000 m and longitude band from the coast to 130°E at 7°N. The annual mean value has been removed before plotting. Positive values represent northward flow.

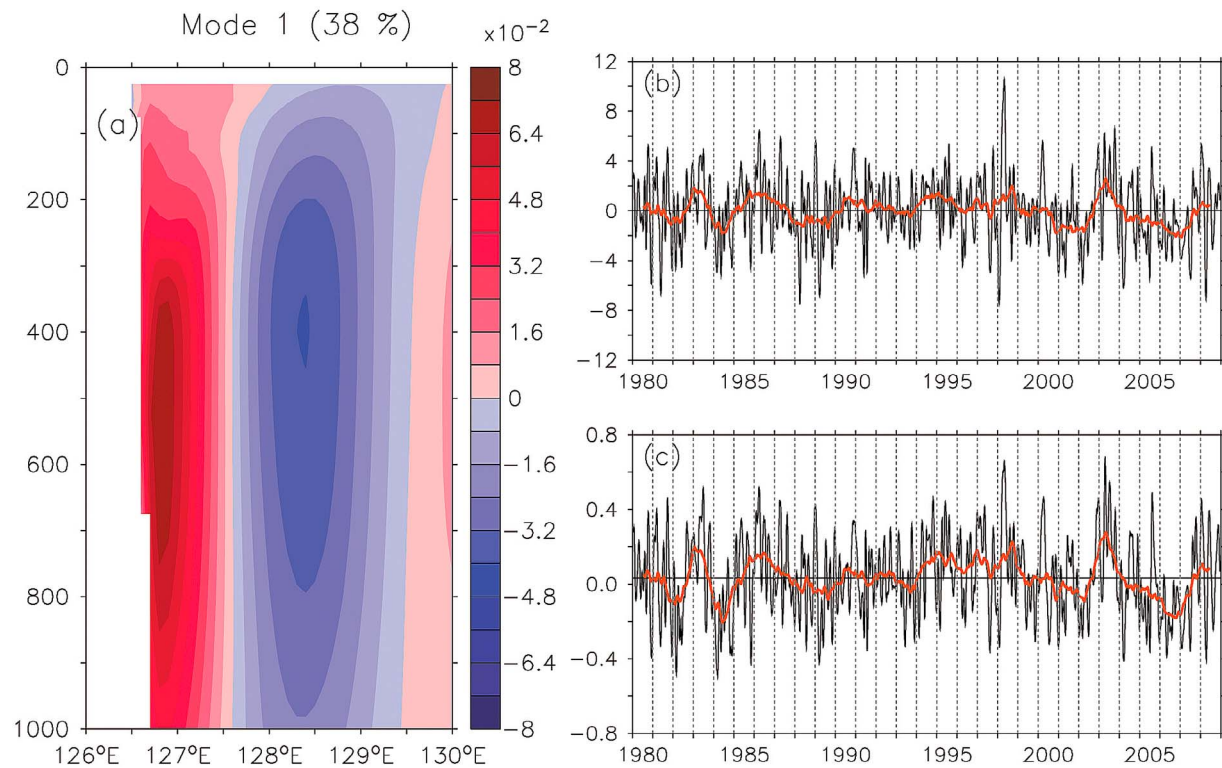


Figure 7. (a) Spatial pattern and (b) corresponding time series of the first EOF mode computed from the meridional velocity at 7°N. (c) Variability (m s^{-1}) in the inshore velocity core of the MUC as indicated by P1 in Figure 3. Red lines show the time series smoothed by a 13-month running mean filter.

shifts of the current (Figure 7b). Its temporal correlation with the inshore velocity core of the MUC exceeds 0.87, which is significant at the 99% confidence level for the entire period of integration (Figure 7c). Interestingly, the correlation of the PC_1 with the offshore velocity core of the MUC is very low ($r = -0.2$), suggesting that the two velocity cores of the MUC are controlled by different processes.

[23] The second EOF mode captures about 22% of the variance, and shows a similar meandering pattern as the first mode, except for an eastward shift by about 1° longitude (Figure 8a). Anti-phase variations are seen on two sides of the zero line approximately lying at 128.5°E , and the positive and negative maxima are located at about 127.7°E and 129.5°E , respectively. The time series of this mode also shows rapid and large onshore/offshore shifts of the current (Figure 8b). Its temporal correlation with the offshore velocity core of the MUC reaches 0.83, satisfying the 99% confidence level. Again, as one would expect from the above analysis, the correlation between PC_2 and the inshore velocity core of the MUC is very close to zero. A positive value of this PC represents a meandering of the current toward the offshore velocity core of the MUC, and vice versa.

[24] The variance conserving spectra of the first two PCs are calculated and compared with those of variability in the two velocity cores of the MUC (Figure 9). The spectra of both PCs show energy peaks at frequency bands around 50–100 days, though the relative importance among these

energy peaks is slightly different for the two modes. Spectra of variability in the two velocity cores of the MUC show essentially the same pattern as the first two PCs. In both cases, meso-scale eddies dominate the subsurface velocity variability. Note that the meandering of the MUC associated with the first two modes can be caused by eddies both from the east and south. So, an eddy that reaches the offshore velocity core does not necessarily reach the inshore core, and vice versa. This possibly explains why the two meandering modes are nearly independent.

[25] Higher EOF modes are also computed (not shown). As the first two modes explain more than 60% of the total variance, contribution from the higher modes is relatively weak. Of particular interest is a “transport mode” identified as mode 5. As previously noted for the Kuroshio transport east of Taiwan [Zhang *et al.*, 2001], this “transport” mode represents a transport pulse superimposed on the mean velocity structure. Its spatial pattern resembles the mean velocity structure (Figure 3a) in nearly all the details. Since the high variability of the MC is confined to a very narrow longitude band near the surface (Figure 3b), this “transport” mode explains only about 5% of the total variance, in contrast with what has been found for the Kuroshio transport east of Taiwan [Zhang *et al.*, 2001].

5. Momentum Balance

[26] To better understand how the MC/MUC is generated, we examine the momentum balance of the current. In

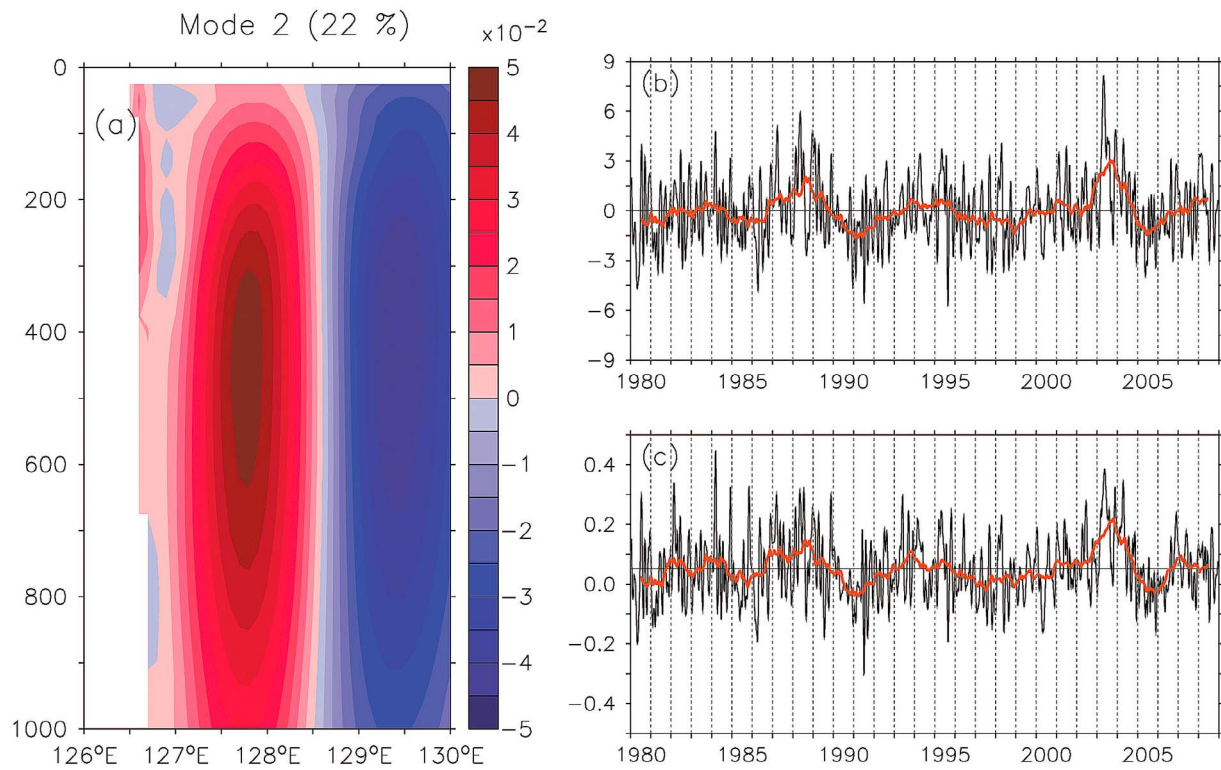


Figure 8. Same as Figure 7 except for the second EOF mode and the variability (m s^{-1}) in the offshore velocity core of the MUC as indicated by P2 in Figure 3.

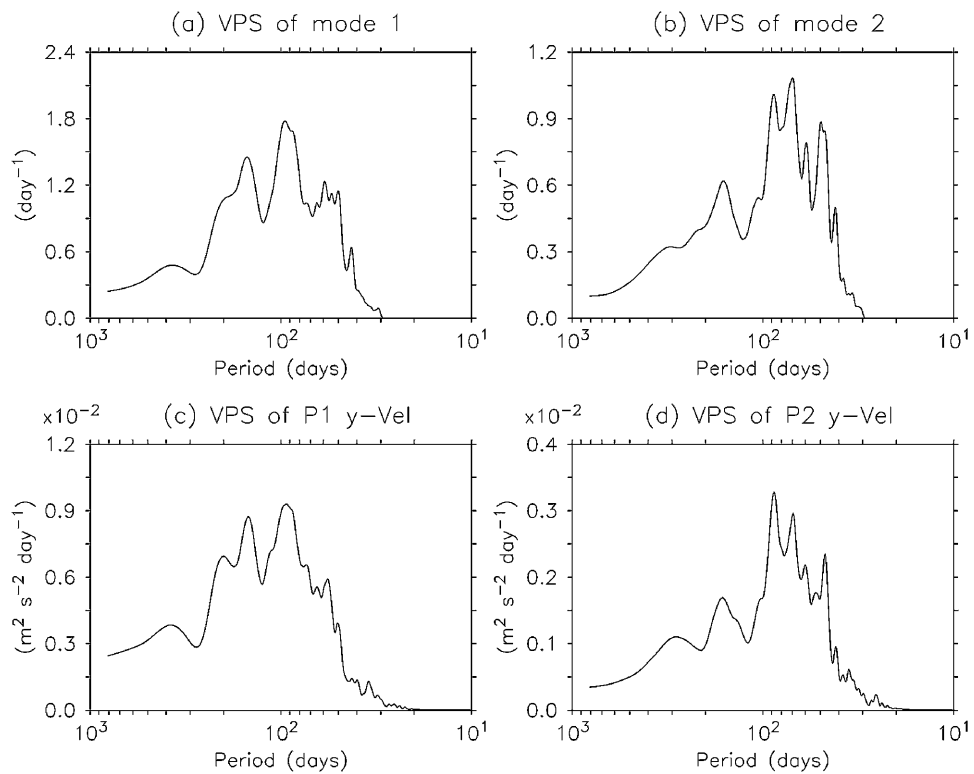


Figure 9. Variance-preserving spectra of the (a) first and (b) second principal component of the EOF compared with those of variability in the (c) inshore (P1) and (d) offshore (P2) velocity cores of the MUC.

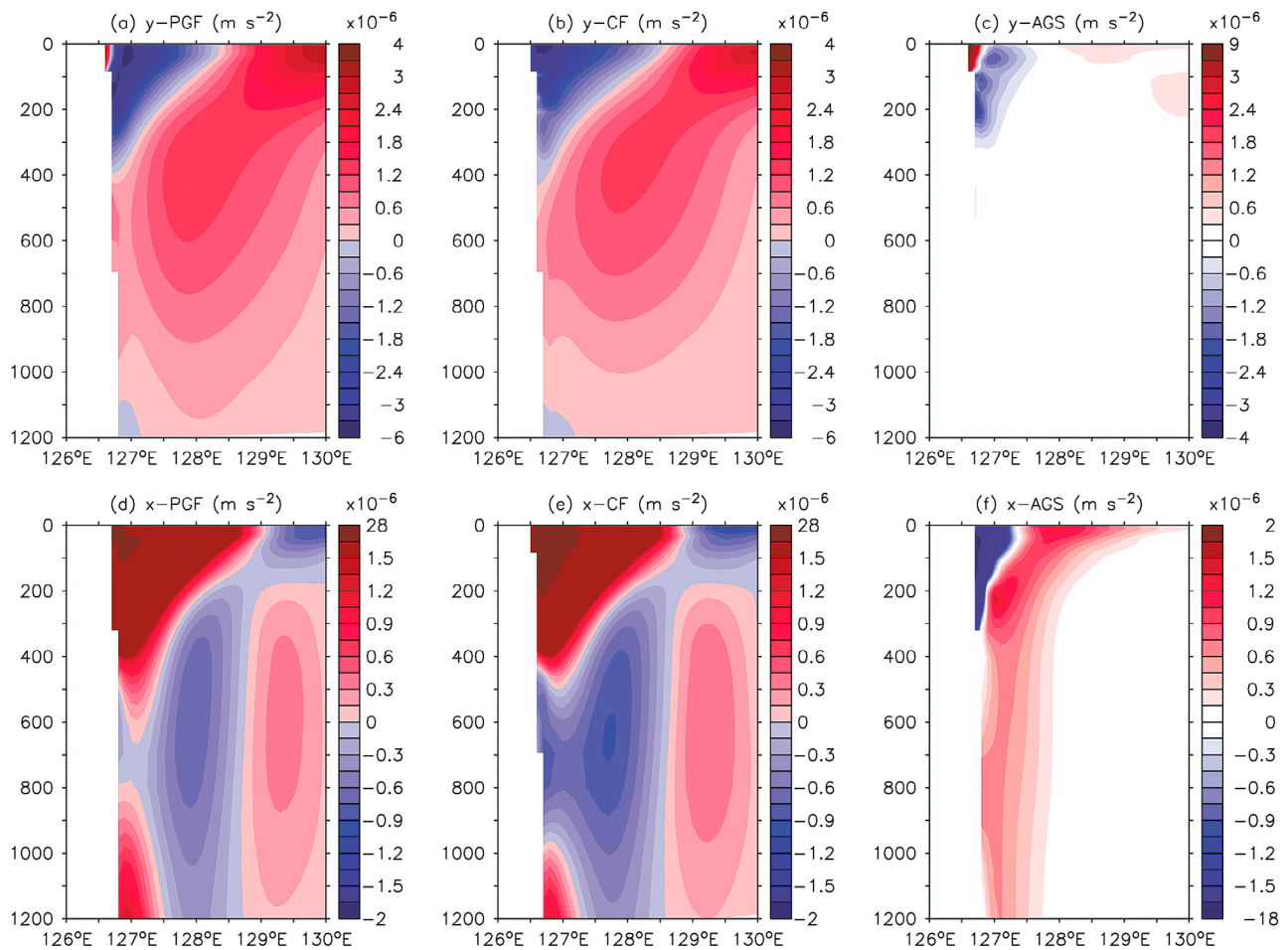


Figure 10. Momentum balance: (a and d) pressure gradient, (b and e) Coriolis force, and (c and f) ageostrophic component in the meridional direction (Figures 10a–10c) and zonal (Figures 10d–10f) direction.

a f -plan, the depth-dependent momentum equations can be written as

$$\frac{\partial u}{\partial t} + u \frac{\partial u}{\partial x} + v \frac{\partial u}{\partial y} + w \frac{\partial u}{\partial z} - fv = -\frac{1}{\rho} \frac{\partial p}{\partial x} + Friction \quad (1)$$

$$\frac{\partial v}{\partial t} + u \frac{\partial v}{\partial x} + v \frac{\partial v}{\partial y} + w \frac{\partial v}{\partial z} + fu = -\frac{1}{\rho} \frac{\partial p}{\partial y} + Friction, \quad (2)$$

where ρ is water density, f is the Coriolis parameter, t is time, and u , v , and w are velocities in the x (eastward), y (northward), and z (upward) directions, respectively. The first term on the left hand side of the equations represents the rate of momentum change (acceleration), the second-to-fourth terms are the momentum advection, and the fifth term is the Coriolis force. The first term on the right hand side represents the pressure gradient. Friction terms, representing a combined effect of wind, diffusion, and sub-grid scale processes, are not readily available and simply regarded as residuals in the present study.

5.1. Mean Balance

[27] All terms except for friction in equations (1) and (2) are first computed using the model's 3-day output, and

then averaged over the entire period of integration (29 years). For the 29 year average, the rate of momentum change is very close to zero and ignored in the following discussion. Because of its nonlinearity, each advection term consists of two components. In the zonal direction, for example, the advection term can be expressed by $\bar{u} \frac{\partial \bar{u}}{\partial x} + \bar{v} \frac{\partial \bar{u}}{\partial y} + \bar{w} \frac{\partial \bar{u}}{\partial z}$ and $u' \frac{\partial u'}{\partial x} + v' \frac{\partial u'}{\partial y} + w' \frac{\partial u'}{\partial z}$, representing the mean advection and eddy induced momentum flux, respectively. Here, quantities with primes are defined as deviations from the 29-year mean values, and represent the combined effect of meso-scale, seasonal, and interannual fluctuations.

[28] Figure 10 shows the momentum balance of the mean current at 7°N. As one can see from this figure, the pressure gradient is primarily balanced by the Coriolis force in both directions. In the meridional direction (Figures 10a and 10b), for example, the two terms resemble each other in nearly all the details across the section, suggesting that the zonal flow is essentially a geostrophic current. The westward flow near the surface causes water to pile up toward the coast. This then creates an eastward directed cross-shelf pressure gradient (Figure 10d) that drives the southward-flowing MC via geostrophy (Figure 10e, $-fv$). Since the zonal flow satisfies

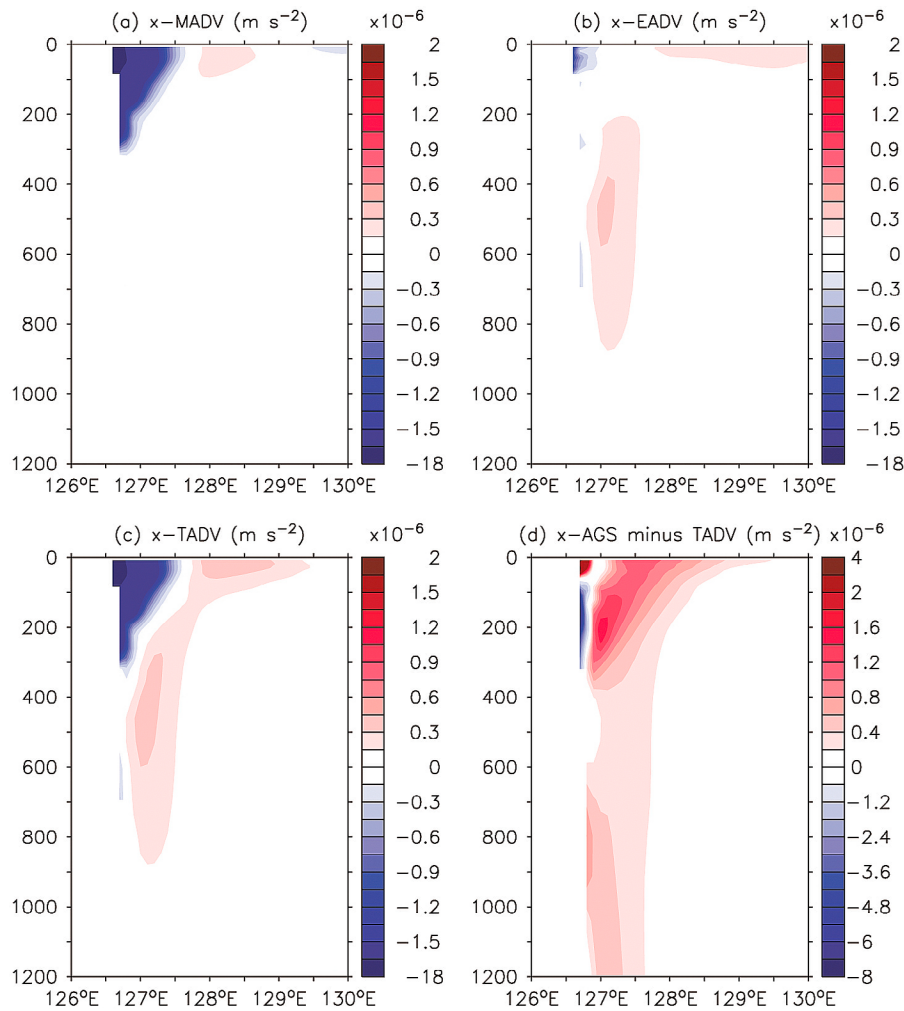


Figure 11. Momentum balance in the zonal direction: (a) mean advection, (b) eddy-induced advection, (c) total advection, and (d) the difference between ageostrophic component and total advection.

the condition of zero transport across the coast, water accumulated near the surface has to be balanced by a return (eastward) flow in the subthermocline (Figure 9b, fu). In response, a northward directed pressure gradient is set up, extending from about 400 m to at least 1000 m, to geostrophically balance the eastward flow off the Mindanao (Figure 9b, fu). The action of this northward directed pressure gradient can be split into two parts. In addition to a geostrophic balance with the eastward flow, it also drives a northward flow (i.e., the MUC) against friction on the inshore edge of the western boundary (Figure 10e, $-fv$). At the same time, the eastward flow (Figure 10b, fu) lifts the isohalines and consequently the isopycnals on the inshore edge (Figure 3c), which then sets up a westward directed cross-shelf pressure gradient to geostrophically balance the Coriolis force associated with the MUC.

[29] The geostrophic balance breaks down on the inshore edge of the western boundary. In the zonal direction (Figure 10f), though the Coriolis force and pressure gradient show essentially the same pattern (Figures 10d and 10e), significant discrepancies can be identified (Figure 10f). Averaged within 1° longitude of the Mindanao coast, these discrepancies account for about 20% of the total momentum

flux at depths near 100 m, indicating that the MC is primarily a geostrophic flow. Ageostrophic component becomes increasingly important with depth and can explain up to 50% of the total momentum flux on the inshore edge of the MUC at depths around 605 m (Figure 10f). Some of this ageostrophic component is related to advection, in which eddy-induced momentum flux seems to be dominant (Figures 11a–11c). Adding the advection term better explains the momentum balance of the MUC. The unexplained portion reflects the influence of friction or a combined effect of wind, diffusion, and sub-grid scale processes near the lateral boundary (Figure 11d).

[30] The offshore velocity core of the MUC is likely related to the intrusion of South Pacific water. In the upper ocean, the Indonesian Throughflow draws water out of the Pacific via the MC. As a consequence, water of South Pacific origin crosses the equator in the deeper layer to conserve mass in the North Pacific, which is a semi-closed basin except for a minor water exchange through the Bering Strait [McCreary *et al.*, 2007]. The inter-hemisphere water exchange mostly occurs in the far western Pacific as part of the NGCUC [Reid, 1965; Lindstrom *et al.*, 1987; Tsuchiya, 1991; Qu *et al.*, 1999], though an interior pathway has also

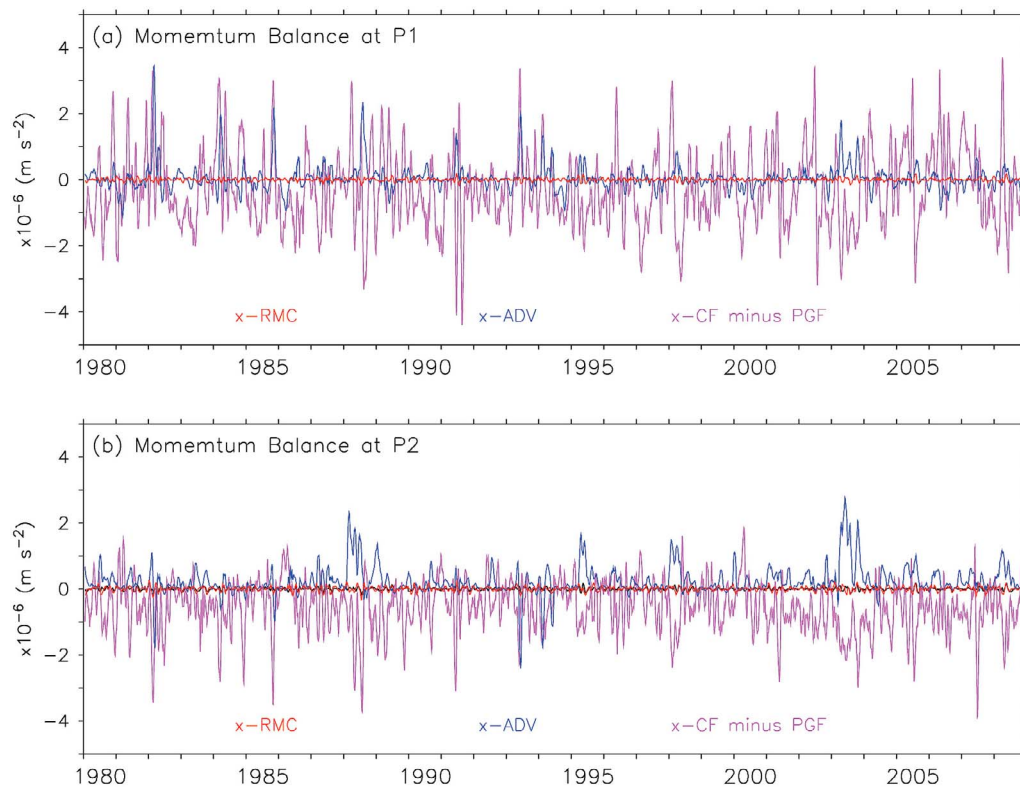


Figure 12. Time series of the rate of momentum change (RMC), advection (ADV), and the difference between Coriolis force (CF) and pressure gradient (PG) in the zonal direction at (a) the inshore and (b) offshore velocity cores of the MUC. The locations of the two cores are marked as P1 and P2 in Figure 3. A 30-day-low-pass filter was applied before plotting.

been identified [e.g., *Johnson and McPhaden, 1999*]. In the subthermocline, when the fresher South Pacific water reaches the southeastern tip of Mindanao, its contrast with the high salinity water from the Sulawesi Sea forms a weak salinity/density front in about 1° longitude of the Mindanao coast (Figure 3c), with relatively high salinity/density water on the inshore side and relatively low salinity/density water on the offshore side of the front. This salinity/density front then sets up a cross-shelf pressure or dynamic height gradient toward the coast (Figure 10d), which in turn generates a northward flow by geostrophy on the offshore edge of the western boundary. Careful examination of momentum balance indicates that approximately 70% of the offshore velocity core of the MUC is in geostrophic balance (Figure 10f). Of the remaining ageostrophic contribution a significant portion can be explained by eddy-induced momentum flux (Figure 11).

5.2. Time Variability

[31] Time series of the rate of momentum change, advection, and difference between Coriolis force and pressure gradient in the zonal direction are presented to illustrate how the MUC is modulated at P₁ and P₂ (marked in Figure 3c) by different processes during the period of integration (Figure 12). As one would expect, the lowest order governing the flow is geostrophy, that is, the balance between Coriolis force and pressure gradient. For the period of integration, the two time series are nearly identical (figure not shown), with their correlation exceeding 0.92 in both

velocity cores of the MUC. On close inspection, one can see significant discrepancies between the two terms in some particular occasions (Figure 12). These discrepancies reflect the influence of ageostrophic processes, and are largely due to advection, in which time variable circulation and/or meso-scale eddies seem to be dominant. Adding advection to the geostrophic balance explains nearly all the momentum variability. Friction as a residual term of equation (1) remains almost unchanged and does not appear to play a significant role in the MUC variability.

6. Effect of Eddies

[32] The above analysis clearly demonstrates that meso-scales (50–100 days) are most energetic time scales of variability in the MC/MUC. Earlier observations have shown evidence that subthermocline eddies exist near the Mindanao coast [*Wijffels et al., 1995; Firing et al., 2005; Kashino et al., 2005*]. The large STDs both in velocity and salinity fields from the model (Figure 3) lend additional support for the existence of subthermocline eddies there. These subthermocline eddies are mostly invisible at the sea surface but may significantly affect the heat, freshwater, and other ocean property transports [e.g., *Firing et al., 2005*].

[33] In the subthermocline, water of South Pacific origin once it crosses the equator in the far western Pacific is characterized by low salinity and high oxygen concentration [e.g., *Reid, 1965*]. The role of the MUC in conveying this low-salinity, high oxygen water toward the western North

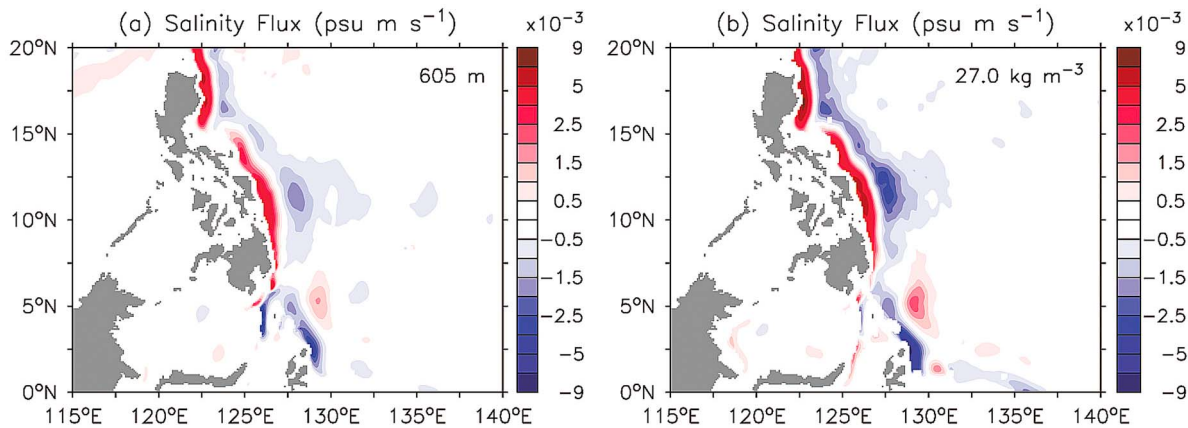


Figure 13. Eddy induced salinity flux, $\overline{v'S'}$, in 10^{-3} psu m s $^{-1}$ at (a) 605 m and (b) $\sigma_{\theta} = 27.0$ kg m $^{-3}$ surface. Positive values indicate northward salinity fluxes or, equivalently, southward freshwater fluxes.

Pacific has been discussed in prior studies [e.g., *Hu et al.*, 1991; *Fine et al.*, 1994; *Wang and Hu*, 1997; *Qu and Lindstrom*, 2004]. An unresolved issue is whether the MUC continues to flow northward along the Philippine coast. Existing observations suggest that in the mean the MUC can only reach about 12°N [e.g., *Hu and Cui*, 1991; *Qu et al.*, 1999] before it turns eastward into the interior ocean [*Hu and Cui*, 1991; *Wang et al.*, 1998]. Farther to the north, the flow below about 500 m is actually dominated by a southward flow (i.e., LUC) [*Qu et al.*, 1997]. The question which may arise immediately is how to explain the low-salinity, high oxygen features observed near the Philippine coast [*Reid*, 1965]. We address this question below by examining the effect of eddies on salinity flux.

[34] In the meridional direction, the gross effect of eddies on salinity flux can be expressed by $\overline{v'S'} = \frac{1}{T} \int_0^T v'S' dt$, where, v' and S' represent deviations of meridional velocity and salinity from their 29-year mean values, respectively. Based on the model's 3-day output, this value (called eddy induced salinity flux hereinafter) is calculated for the entire 29 years. The result clearly shows an eddy-induced northward salinity flux on the inshore edge and an eddy induced southward salinity flux on the offshore edge of the western boundary (Figure 13). The northward flux seems to originate from the Sulawesi Sea, where salinity is higher than the Pacific side (Figure 3), and is likely related to the inshore velocity core of the MUC. With a northward directed salinity gradient on the inshore edge (Figure 2), eddies take relatively high salinity water to the north and relatively low salinity water to the south, with their gross effect generating a northward salinity flux (Figure 13). The situation on the offshore edge looks different, where a southward salinity flux, or equivalently a northward freshwater flux, is seen extending from the New Guinea coast all the way to the Luzon Strait. It attains its maximum value ($\sim 7 \times 10^{-3}$ psu m s $^{-1}$) at 10°N–12°N, roughly coinciding with the maximum velocity variability there (Figure 2b). In the lower latitudes, approximately south of 10°N–12°N, there is a southward directed salinity gradient in the mean (Figure 2c). An ensemble of eddies provides an additional advection of freshwater to the mean advection by the NGCUC and MUC. In the higher latitudes, approximately north of 10°N–12°N, the mean

salinity gradient on the offshore edge becomes northward, but the eddy induced freshwater flux remains northward, in an opposite direction to the advection by the mean current (i.e., the LUC).

[35] Note that, by the above definition, eddy induced freshwater flux contains contribution both from seasonal and interannual variations, which is generally small relative to the effect of meso-scale fluctuations. On the offshore edge of the MUC at 7°N, for example, more than 70% of the eddy-induced freshwater flux is due to meso-scale fluctuations. Further inspection of the result indicates that the eddy induced freshwater flux attains its maximum of about 4.7×10^{-4} psu m s $^{-1}$ at about 600 m there (Figure 14). Averaged over the longitude band between 127.0°E and 128.5°E, roughly coinciding with the offshore velocity core of the MUC, this northward freshwater flux reaches about 2.3×10^{-4} psu m s $^{-1}$. A useful quantity to measure such eddy effect is the “bolus” velocity, which has been extensively used in prior studies [*Marshall*, 1997]. We define the “bolus” velocity in the present study by $\langle v'S' \rangle / \Delta S$, where ΔS represents the salinity difference between the North and South Pacific waters being converged in the western tropical Pacific. As an example, ΔS is calculated as the difference between 8°N and 6°N along 127.7°E, approximately coinciding with the northern and southern edge of the Mindanao Eddy, respectively. In the density range between 26.9 and 27.3 kg m $^{-3}$, the mean ΔS simulated by the model is about 16×10^{-4} psu. This salinity difference yields a “bolus” velocity estimate of about 0.3 m s $^{-1}$, greater than the mean MUC by a factor of 6. So, to a certain extent, eddy-induced freshwater flux explains why South Pacific water appears to extend farther northward than the mean MUC along the offshore edge of the western boundary [e.g., *Qu et al.*, 1999]. Its impact on salinity budget of the region needs to be investigated further by research.

7. Summary and Discussion

[36] Analysis of results from OFES showed two sub-thermocline velocity cores in the mean off the Mindanao coast, both of which are referred to as the MUC in the present study. The inshore velocity core hugs the coast near 126.8°E at 7°N. Part of this velocity core can be traced to the

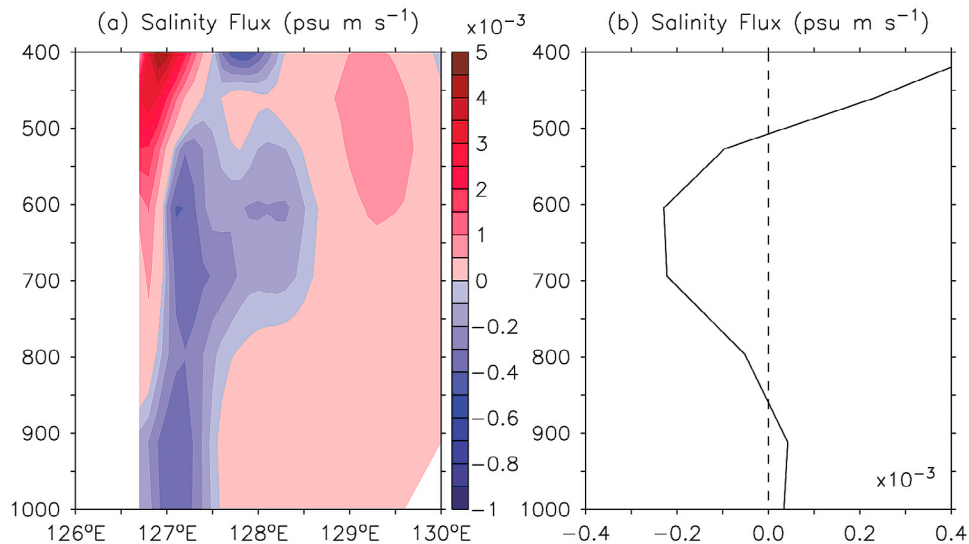


Figure 14. (a) Eddy-induced salinity flux, $\overline{v'S'}$, in 10^{-3} psu $m s^{-1}$, and (b) vertical profile of the flux averaged between 127°E and 128.5°E along 7°N.

Sulawesi Sea along the Mindanao coast, where salinity in the subthermocline is relatively high. The offshore velocity core takes place at about 127.7°E. Water associated with this velocity core is primarily of South Pacific origin. The model results confirm that the MUC is weak in the mean (~ 0.05 $m s^{-1}$), being considerably smaller than its variability (up to 0.20 $m s^{-1}$); but, it tends to exist during all the period of integration. Its distinctive water properties suggest that the current has a South Pacific origin and cannot be merely a component of local recirculation or eddies. We note that the inshore velocity core of the MUC was not markedly evident in earlier hydrographic observations [e.g., *Qu et al.*, 1998], presumably due to the coarse space resolution of the data, as well as due to the barotropic component of the current resulting from the cross-shelf sea surface height gradient and the reference level velocity [*Firing et al.*, 2005].

[37] The most energetic time scale of variability in the MC/MUC is 50–100 days. EOF analysis suggests that approximately 60% of the total variance over the 0–1000 m depth range can be explained by the first two modes. Both modes represent meandering motions in the subthermocline. The first mode corresponds well with the inshore velocity core of the MUC, while the second meandering mode is closely related to the offshore velocity core of the MUC. The first two principal components also show a variability dominated by fluctuations on time scales of 50–100 days. The meandering caused by the arrival of meso-scale eddies can significantly alter the structure and transport of the MUC.

[38] Mean momentum balance in the MC/MUC shows that the Coriolis force and pressure gradient are the dominant forces, suggesting that the MC/MUC is approximately a geostrophic flow. Ageostrophic dynamics becomes important in the subthermocline. Our analysis suggests that approximately 50% of the inshore velocity core of the MUC can be explained by ageostrophic dynamics. This result could be interpreted as another reason why the inshore velocity core of the MUC was relatively weak in earlier

hydrographic observations. The offshore velocity core of the MUC is likely related to the intrusion of freshwater from the South Pacific. Being about 100 km away from the lateral boundary, at least 70% of this velocity core is in geostrophic balance. Time series of momentum balance shows a good coherence between the Coriolis force and pressure gradient in the MUC, with a correlation exceeding 0.92 in both cores. We emphasize that, though closely related, the two velocity cores of the MUC are likely governed by different processes.

[39] Eddy activities can produce significant salinity fluxes that cannot be explained by the mean current. Our analysis clearly shows the existence of an eddy-induced freshwater flux along the offshore edge of the western boundary, extending from the New Guinea coast all the way to the Luzon Strait. This eddy induced northward freshwater flux provides additional advection to the mean current south of about 12°N, but acts as the only pathway for South Pacific water to extend further northward. In the MUC, a “bolus” velocity is identified, which can be as large as 0.3 $m s^{-1}$ in the AAIW density range between 26.9 and 27.3 $kg m^{-3}$. This “bolus” velocity is greater than the mean MUC by a factor of 6. We note that, since the low salinity signal of South Pacific origin is weak, there is no easy way to trace this signal after it reaches about 12°N along the Philippine coast [*Qu et al.*, 1999]. It is highly possible that the low-salinity signal is gradually mixed away as it propagates farther northward. The impact of the eddy-induced northward freshwater flux on the region’s salinity distribution can be identified by a detailed salinity budget analysis. We will leave this for a future study.

[40] Yet, it still remains unknown where the energetic meso-scale eddies originate and how they are dissipated in the far western Pacific. As velocity structure in the subthermocline bears little resemblance to that near the surface, *Firing et al.* [2005] suggested that the energy source of these eddies cannot be local wind-forcing or instability of upper-layer currents. *Dutrieux* [2009] attributed these eddies to the baroclinic instability of subthermocline currents. Indeed, careful examination of velocity structure from the model

shows strong velocity shears in the subthermocline. The generation of meso-scale eddies could be related to the instability of the lower parts of the NEC, NECC, and NGCUC, and the details need to be investigated further by research.

[41] **Acknowledgments.** This research was supported by NSF through grant OCE10-29704 and by JAMSTEC, NASA, and NOAA through their sponsorship of research activities at the International Pacific Research Center (IPRC). Additional support for T.-L. Chiang was provided by NSC 100-2811-M-003-013. C.-R. Wu was supported by NSC 100-2628-M-003-001. P. Dutrieux was supported by NSF through grant OCE05-50857. D. Hu was supported by NSFC major project 40890151 and MOST 2012CB417401. The authors are grateful to K. Richards, B. Qiu, E. Firing, R. Lukas, R. Fine, and E. J. Lindstrom for useful communications on the topic, to H. Sasaki and colleagues from the Earth Simulator for assistance in processing the OFES outputs, and to the three anonymous reviewers for thoughtful comments on an earlier version of the manuscript. School of Ocean and Earth Science and Technology contribution 8682, and International Pacific Research Center contribution IPRC-890.

References

- Bingham, F. M., and R. Lukas (1995), The distribution of intermediate water in the western equatorial Pacific during January–February 1986, *Deep Sea Res., Part I*, 42(9), 1545–1573, doi:10.1016/0967-0637(95)00064-D.
- Chelton, D. B., M. G. Schlax, R. M. Samelson, and R. A. de Szoeke (2007), Global observations of large oceanic eddies, *Geophys. Res. Lett.*, 34, L15606, doi:10.1029/2007GL030812.
- Dutrieux, P. (2009), Tropical western Pacific currents and the origin of intraseasonal variability below the thermocline, PhD thesis, 140 pp., Univ. of Hawai'i at Mānoa, Honolulu.
- Fine, R. A., R. Lukas, F. M. Bingham, M. J. Warner, and R. H. Gammon (1994), The western equatorial Pacific is a water mass crossroads, *J. Geophys. Res.*, 99(C12), 25,063–25,080, doi:10.1029/94JC02277.
- Firing, E., Y. Kashino, and P. Hacker (2005), Energetic subthermocline currents observed east of Mindanao, *Deep Sea Res., Part II*, 52(3–4), 605–613, doi:10.1016/j.dsr2.2004.12.007.
- Hsin, Y.-C., T. Qu, and C.-R. Wu (2010), Intra-seasonal variation of the Kuroshio southeast of Taiwan and its possible forcing mechanism, *Ocean Dyn.*, 60(5), 1293–1306, doi:10.1007/s10236-010-0294-2.
- Hu, D., and M. Cui (1989), The western boundary current in the far-western Pacific Ocean, in *Proceedings of Western Pacific International Meeting and Workshop on TOGA-COARE, May 24–30, 1989, Nouméa, New Caledonia*, edited by J. Picaut, R. Lukas, and T. Delcroix, pp. 123–134, Inst. Fr. de Rech. Sci. pour le Dév. en Coop., Nouméa.
- Hu, D., and M. Cui (1991), The western boundary current of the Pacific and its role in the climate, *Chin. J. Oceanol. Limnol.*, 9, 1–14, doi:10.1007/BF02849784.
- Hu, D., M. Cui, T. Qu, and Y. Li (1991), A subsurface northward current off Mindanao identified by dynamic calculation, in *Oceanography of Asian Marginal Seas, Elsevier Oceanogr. Ser.*, vol. 54, edited by K. Takano, pp. 359–365, Elsevier, Amsterdam, doi:10.1016/S0422-9894(08)70108-9.
- Johns, W. E., T. N. Lee, D. Zhang, R. Zantopp, C.-T. Liu, and Y. Yang (2001), The Kuroshio east of Taiwan: Moored transport observations from the WOCE PCM-1 array, *J. Phys. Oceanogr.*, 31(4), 1031–1053, doi:10.1175/1520-0485(2001)031<1031:TKEOTM>2.0.CO;2.
- Johnson, G. C., and M. J. McPhaden (1999), Interior pycnocline flow from the subtropical to the equatorial Pacific Ocean, *J. Phys. Oceanogr.*, 29(12), 3073–3089, doi:10.1175/1520-0485(1999)029<3073:IPFFTS>2.0.CO;2.
- Kashino, Y., H. Watanabe, B. Herunadi, M. Aoyama, and D. Hartoyo (1999), Current variability at the Pacific entrance of the Indonesian throughflow, *J. Geophys. Res.*, 104(C5), 11,021–11,035, doi:10.1029/1999JC000033.
- Kashino, Y., A. Ishida, and Y. Kuroda (2005), Variability of the Mindanao Current: Mooring observation results, *Geophys. Res. Lett.*, 32, L18611, doi:10.1029/2005GL023880.
- Kashino, Y., N. España, F. Syamsudin, K. J. Richards, T. Jensen, P. Dutrieux, and A. Ishida (2009), Observations of the North Equatorial Current, Mindanao Current, and the Kuroshio Current system during the 2006/07 El Niño and 2007/08 La Niña, *J. Oceanogr.*, 65(3), 325–333, doi:10.1007/s10872-009-0030-z.
- Kashino, Y., A. Ishida, and S. Hosoda (2011), Observed ocean variability in the Mindanao Dome region, *J. Phys. Oceanogr.*, 41(2), 287–302, doi:10.1175/2010JPO4329.1.
- Kessler, W. S. (1990), Observations of long Rossby waves in the northern tropical Pacific, *J. Geophys. Res.*, 95(C4), 5183–5217, doi:10.1029/JC095iC04p05183.
- Kessler, W. S. (2005), The oceans, in *Intraseasonal Variability in the Atmosphere-Ocean Climate System*, edited by W. K. M. Lau and D. E. Waliser, pp. 175–222, Springer, New York, doi:10.1007/3-540-27250-X_6.
- Kim, Y. Y., T. Qu, T. Jensen, T. Miyama, H. Mitsudera, H.-W. Kang, and A. Ishida (2004), Seasonal and interannual variations of the NEC bifurcation in a high-resolution OGCM, *J. Geophys. Res.*, 109, C03040, doi:10.1029/2003JC002013.
- Lee, T., W. Johns, C.-T. Liu, D. Zhang, R. Zantopp, and Y. Yang (2001), Mean transport and seasonal cycle of the Kuroshio east of Taiwan with comparison to the Florida Current, *J. Geophys. Res.*, 106(C10), 22,143–22,158, doi:10.1029/2000JC000535.
- Lindstrom, E., R. Lukas, R. Fine, E. Firing, S. J. Godfrey, G. Meyers, and M. Tsuchiya (1987), The western equatorial Pacific Ocean circulation study, *Nature*, 330, 533–537, doi:10.1038/330533a0.
- Lukas, R. (1988), Interannual fluctuations of the Mindanao Current inferred from sea level, *J. Geophys. Res.*, 93(C6), 6744–6748, doi:10.1029/JC093iC06p06744.
- Lukas, R., E. Firing, P. Hacker, P. L. Richardson, C. A. Collins, R. Fine, and R. Gammon (1991), Observations of the Mindanao Current during the Western Equatorial Pacific Ocean Circulation Study, *J. Geophys. Res.*, 96(C4), 7089–7104, doi:10.1029/91JC00062.
- Lukas, R., T. Yamagata, and J. P. McCreary (1996), Pacific low-latitude western boundary currents and the Indonesian throughflow, *J. Geophys. Res.*, 101(C5), 12,209–12,216, doi:10.1029/96JC01204.
- Madden, R. A., and P. R. Julian (1994), Observations of the 40–50 day tropical oscillation: A review, *Mon. Weather Rev.*, 122(5), 814–837, doi:10.1175/1520-0493(1994)122<0814:OOTDTP>2.0.CO;2.
- Marshall, D. (1997), Subduction of water masses in an eddying ocean, *J. Mar. Res.*, 55(2), 201–222, doi:10.1357/0022240973224373.
- Masumoto, Y., and T. Yamagata (1991), Response of the western tropical Pacific to the Asian winter monsoon: The generation of the Mindanao Dome, *J. Phys. Oceanogr.*, 21(9), 1386–1398, doi:10.1175/1520-0485(1991)021<1386:ROTWTP>2.0.CO;2.
- Masumoto, Y., et al. (2004), A fifty-year eddy-resolving simulation of the world ocean—Preliminary outcomes of OFES (OGCM for the Earth simulator), *J. Earth Simul.*, 1, 35–56.
- McCreary, J. P., T. Miyama, R. Furue, T. Jensen, H.-W. Kang, B. Bang, and T. Qu (2007), Interactions between the Indonesian Throughflow and circulations in the Indian and Pacific Oceans, *Prog. Oceanogr.*, 75(1), 70–114, doi:10.1016/j.pocan.2007.05.004.
- Nitani, H. (1972), Beginning of the Kuroshio, in *Kuroshio: Physical Aspects of the Japan Current*, edited by H. Stommel and K. Yoshida, pp. 129–163, Univ. of Wash. Press, Seattle.
- Qiu, B., and R. Lukas (1996), Seasonal and interannual variability of the North Equatorial Current, the Mindanao Current, and the Kuroshio along the Pacific western boundary, *J. Geophys. Res.*, 101(C5), 12,315–12,330, doi:10.1029/95JC03204.
- Qiu, B., M. Mao, and Y. Kashino (1999), Intraseasonal variability in the Indo-Pacific throughflow and the region surrounding the Indonesian Seas, *J. Phys. Oceanogr.*, 29(7), 1599–1618, doi:10.1175/1520-0485(1999)029<1599:IVITIP>2.0.CO;2.
- Qu, T., and E. J. Lindstrom (2004), Northward intrusion of the Antarctic Intermediate Water in the western Pacific, *J. Phys. Oceanogr.*, 34(9), 2104–2118, doi:10.1175/1520-0485(2004)034<2104:NIOAIW>2.0.CO;2.
- Qu, T., and R. Lukas (2003), The bifurcation of the North Equatorial Current in the Pacific, *J. Phys. Oceanogr.*, 33(1), 5–18, doi:10.1175/1520-0485(2003)033<0005:TBOTNE>2.0.CO;2.
- Qu, T., T. Kagimoto, and T. Yamagata (1997), A subsurface countercurrent along the east coast of Luzon, *Deep Sea Res., Part I*, 44(3), 413–423, doi:10.1016/S0967-0637(96)00121-5.
- Qu, T., H. Mitsudera, and T. Yamagata (1998), On the western boundary currents in the Philippine Sea, *J. Geophys. Res.*, 103(C4), 7537–7548, doi:10.1029/98JC00263.
- Qu, T., H. Mitsudera, and T. Yamagata (1999), A climatology of the circulation and water mass distribution near the Philippine coast, *J. Phys. Oceanogr.*, 29(7), 1488–1505, doi:10.1175/1520-0485(1999)029<1488:ACOTCA>2.0.CO;2.
- Qu, T., J. Gan, A. Ishida, Y. Kashino, and T. Tozuka (2008), Semiannual variation in the western tropical Pacific Ocean, *Geophys. Res. Lett.*, 35, L16602, doi:10.1029/2008GL035058.
- Reid, J. L., Jr. (1965), *Intermediate Waters of the Pacific Ocean, Johns Hopkins Oceanogr. Stud. Ser.*, vol. 2, 85 pp., Johns Hopkins Press, Baltimore, Md.
- Sasaki, H., Y. Sasai, S. Kawahara, M. Furuichi, F. Araki, A. Ishida, Y. Yamanaka, Y. Masumoto, and H. Sakuma (2004), A series of eddy-

- resolving ocean simulations in the world ocean: OFES (OGCM for the Earth Simulator) project, in *OCEAN'04. MITS/IEEE TECHNO-OCEAN '04*, vol. 3, pp. 1535–1541, Inst. of Electr. and Electron. Eng., New York, doi:10.1109/OCEANS.2004.1406350.
- Toole, J. M., R. C. Millard, Z. Wang, and S. Pu (1990), Observations of the Pacific North Equatorial Current bifurcation at the Philippine coast, *J. Phys. Oceanogr.*, *20*(2), 307–318, doi:10.1175/1520-0485(1990)020<0307:OOTPNE>2.0.CO;2.
- Tozuka, T., T. Kagimoto, Y. Masumoto, and T. Yamagata (2002), Simulated multiscale variations in the western tropical Pacific: The Mindanao Dome revisited, *J. Phys. Oceanogr.*, *32*(5), 1338–1359, doi:10.1175/1520-0485(2002)032<1338:SMVITW>2.0.CO;2.
- Tsuchiya, M. (1991), Flow path of Antarctic Intermediate Water in the western equatorial South Pacific Ocean, *Deep Sea Res., Part A*, *38*, suppl. 1, S273–S279.
- Wang, F., and D. Hu (1997), A preliminary study on water source of the Mindanao Undercurrent (in Chinese with English abstract), in *Collected Works in Memoriam of Professor Jiuzhang Zhao*, edited by D. Ye, pp. 345–352, Science Press, Beijing.
- Wang, F., and D. Hu (1998a), Dynamic and thermohaline properties of the Mindanao Undercurrent, part I: Dynamic structure, *Chin. J. Oceanol. Limnol.*, *16*(2), 122–127, doi:10.1007/BF02845177.
- Wang, F., and D. Hu (1998b), Dynamic and thermohaline properties of the Mindanao Undercurrent, part II: Thermohaline structure, *Chin. J. Oceanol. Limnol.*, *16*(3), 206–213, doi:10.1007/BF02848724.
- Wang, F., D. Hu, and H. Bai (1998), Western boundary undercurrents east of the Philippines, in *Proceedings of PORSEC '98—Qingdao, 28–31 July 1998*, edited by M.-X. He and G. Chen, pp. 551–556, Ocean Remote Sens. Inst., Ocean Univ. of Qingdao, Qingdao, China.
- Wang, Q., and D. Hu (2006), Bifurcation of the North Equatorial Current derived from altimetry in the Pacific Ocean, *J. Hydrodyn.*, *18*(5), 620–626, doi:10.1016/S1001-6058(06)60144-3.
- Wijffels, S., E. Firing, and J. Toole (1995), The mean structure and variability of the Mindanao Current at 8°N, *J. Geophys. Res.*, *100*(C9), 18,421–18,435, doi:10.1029/95JC01347.
- Wu, C.-R., and T.-L. Chiang (2007), Mesoscale eddies in the northern South China Sea, *Deep Sea Res., Part II*, *54*(14–15), 1575–1588, doi:10.1016/j.dsr2.2007.05.008.
- Wyrtki, K. (1961), Physical oceanography of the Southeast Asian waters, *Naga Rep.* *2*, 195 pp., Scripps Inst. of Oceanogr., La Jolla, Calif.
- Zhang, D., T. N. Lee, W. E. Johns, C.-T. Liu, and R. Zantopp (2001), The Kuroshio east of Taiwan: Modes of variability and relationship to interior mesoscale eddies, *J. Phys. Oceanogr.*, *31*(4), 1054–1074, doi:10.1175/1520-0485(2001)031<1054:TKEOTM>2.0.CO;2.